Structural hormesis in protein aggregation: A minimal mechanistic model

Abhishek Mallela[a], Santiago Schnell[a,b]

[a]*Department of Mathematics, Dartmouth, Hanover, NH 03755, USA*
[b]*Department of Biochemistry & Cell Biology, and Department of Biomedical Data Sciences, Geisel School of Medicine at Dartmouth, Hanover, NH 03755, USA*

Abstract

Protein aggregation underlies the pathogenesis of many neurodegenerative diseases, and inhibitors are often assumed to elicit monotonic dose–responses. We ask whether simple aggregation pathways can *intrinsically* generate hormesis—a biphasic profile with low–dose stimulation and high–dose inhibition. We formulate a minimal mechanistic model in which a single inhibitor interacts sequentially with pathway intermediates. Analysis and simulation show a robust non–monotonic response: low inhibitor doses increase aggregate formation, whereas high doses suppress it. We prove that this profile is structural—arising from chemical network topology rather than tuned kinetic parameters. The mechanism rationalizes pro–aggregating effects at low doses and underscores the need for full–range dose–response evaluation in inhibitor screening.

Keywords: Protein aggregation, Hormesis, Biphasic dose-response, Mathematical modeling, Reaction network topology, Ordinary differential equations, Inhibitor screening

1. Introduction

Protein aggregation—the self–assembly of soluble monomers into larger, often insoluble assemblies—is central to many areas of biology and medicine. It is implicated in numerous debilitating human disorders, including Alzheimer's and Parkinson's diseases, and also poses challenges for the manufacturing and storage of protein therapeutics [1, 2, 3]. A persistent objective in biomedical research is therefore to regulate aggregation kinetics, often with small molecules or biological modulators that inhibit aggregation [4, 5]. In practice, efficacy is typically assessed under the implicit assumption of a monotonic dose–response; yet biological systems frequently violate this assumption [6, 7, 8].

A salient form of non–monotonicity is *hormesis*: stimulation at low doses and inhibition at high doses. Hormetic responses are widely documented across toxicology, pharmacology, ecology, and pest management [6, 8, 9], and have been framed as a "paradox of the dose" with implications for therapy and risk assessment [10]. In systems biology, such biphasic behaviour can arise from *structural* features of chemical network topology (e.g., sequential engagement

Email address: santiago.schnell@dartmouth.edu (Santiago Schnell)

of intermediates, competition for binding sites, or pathway branch points), independently of allostery, substrate inhibition, product activation, or the presence of explicit feedback and feedforward loops [11, 12].

There is growing evidence that hormesis can arise specifically in protein aggregation systems. Mild stressors such as transient heat shock or dietary restriction can reduce aggregation in models of polyglutamine diseases and α–synucleinopathies, whereas higher or chronic exposures are detrimental, often via HSP or Nrf2–mediated proteostasis pathways [13, 14]. Conversely, presumed inhibitors may paradoxically stimulate aspects of aggregation at low concentrations: for example, trehalose can expedite the onset of α–synuclein aggregation while reducing overall fibril load [15], and the small heat–shock protein α–crystallin can accelerate insulin aggregation under particular solution conditions [16]. In the language of our motif, such modulators act as an inhibitor engaging different intermediates with distinct affinities or activities, thereby biasing fluxes through early versus late steps in a concentration–dependent manner.

Mechanistic mathematical modeling is well–suited to disentangle these phenomena: models formulated using ordinary differential equations (ODEs) isolate network components and expose the structural features responsible for paradoxical responses [12, 17, 18]. In a related context, Rashkov et al. [17] showed that inhibition within a signaling cascade can yield hormesis in the pathway output under certain parameter regimes, underscoring the role of network competition and feedback [11]. Protein aggregation kinetics emerge from a hierarchy of coupled microscopic steps—including primary nucleation, elongation, secondary nucleation, and fragmentation—for which mean–field reductions yield tractable ODE models that successfully fit and rationalize macroscopic observables [19, 20, 21, 22, 23, 24]. These frameworks have been used extensively to interpret experiments and extract rate laws across proteins and conditions [3, 23].

In this work, we introduce a minimal phenomenological reaction mechanism of protein aggregation modulated by an inhibitor as a coarse–grained motif, abstracting a richer cascade of intermediates that represent successive pre–fibrillar species along the nucleation/oligomerisation pathway, while the mature aggregate pool collects products of elongation and secondary pathways. We make explicit the assumptions under which this coarse–graining is appropriate—early–time kinetics before substantial monomer depletion, quasi–steady behaviour of rapidly equilibrating steps, and effective rate constants that lump secondary processes. Such coarse-grained representations have proven effective for characterizing aggregation kinetics across diverse protein systems, including amyloid-β, α-synuclein, prions, and insulin, where phenomenological two-step models capture essential features of the aggregation time course despite abstracting over size-distribution dynamics [25, 26]. We develop a minimal mechanistic model in which a *single inhibitor* acts sequentially on pathway intermediates. Using mathematical analysis and computational simulation, we show that the model predicts a robust biphasic response of aggregate abundance over a wide range of kinetic parameters. We further *prove* that this response is structural: it follows from the topology of the reaction network rather than from finely tuned rate constants, where low inhibitor concentrations favor a productive intermediate to increase aggregate production, whereas high concentrations divert flux into an off–pathway sink and reduce aggregation. We conclude by discussing implications for inhibitor screening—including the necessity of full–range dose–response characterization—and for interpreting paradoxical low–dose stimulation in systems

with aggregation.

2. A minimal reaction mechanism of aggregation with inhibition

We present a minimal reaction network based on well-established phenomenological principles of protein aggregation and small-molecule modulation [25, 26]. As shown in FIGURE 1, the reaction scheme begins with the formation of an initial complex, C_1, from soluble monomeric proteins, M. This step represents primary nucleation, a fundamental and rate-limiting process in many aggregation pathways [2, 3]. The on-pathway progression from C_1 to the final aggregate, A, through an intermediate state, C_2, reflects the multistep nature of aggregation, which often involves the formation of structured oligomers and protofibrils prior to the final fibrillar state.

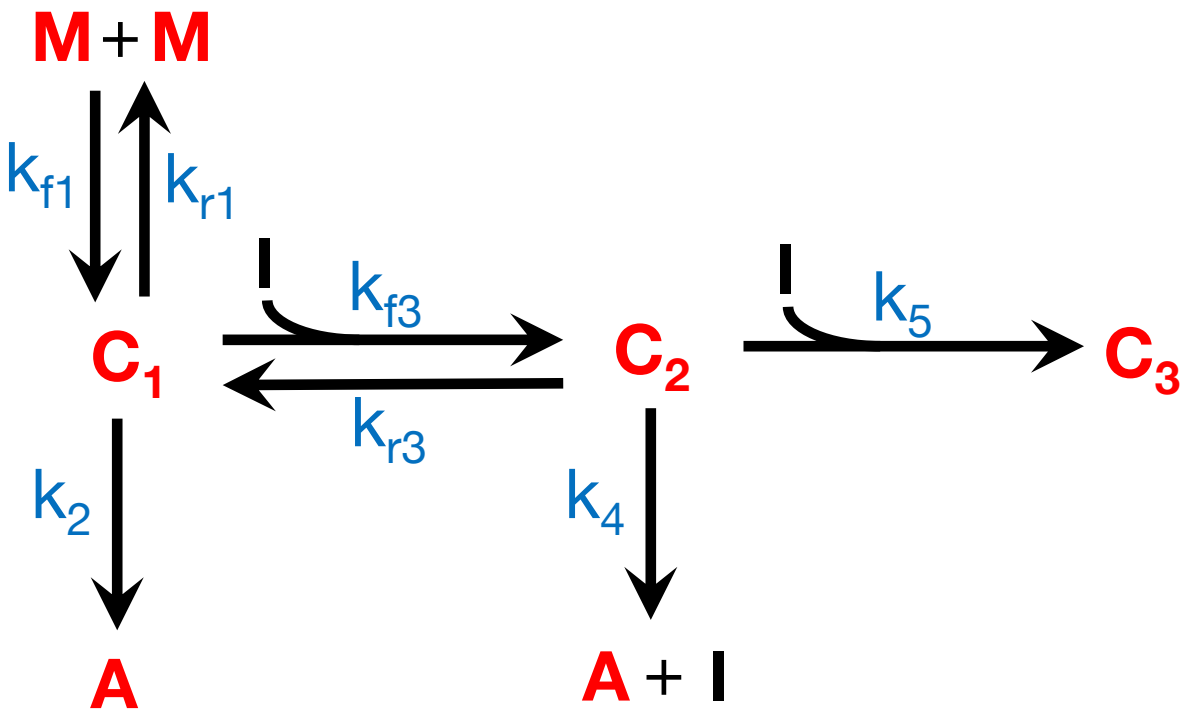

Figure 1: **Schematic of the protein aggregation mechanism.** Monomer M forms the dimeric intermediate C_1, which converts reversibly to C_2 and then to the final aggregate A. The inhibitor I interacts sequentially with intermediates, and an off–pathway sink C_3 is formed at high I via k_5. Rate constants are indicated on the arrows.

The central feature of our model is the dual role of the inhibitor (modulator), I. The modulator's ability to bind the on-pathway intermediates, C_1 and C_2, is mechanistically plausible. At low concentrations, the modulator can promote a productive conformation or nucleation reaction step, consistent with observations of certain small molecules or chaperones that can "prime" a protein for assembly. At higher concentrations, the modulator's interaction with the intermediate C_2 leads to the formation of an inactive complex, C_3.

This sequestration mechanism represents a direct and potent form of inhibition, where the modulator effectively removes productive species from the aggregation pathway.

To investigate the kinetic effects of the inhibitor in this protein aggregation mechanism, we apply the law of mass action to derive the set of ordinary differential equations governing the reactions:

$$\frac{\mathrm{d}[M]}{\mathrm{d}t} = -2k_{f1}[M]^2 + 2k_{r1}[C_1] \tag{1}$$

$$\frac{\mathrm{d}[I]}{\mathrm{d}t} = -k_{f3}[C_1][I] + (k_{r3} + k_4 - k_5[I])[C_2] \tag{2}$$

$$\frac{\mathrm{d}[C_1]}{\mathrm{d}t} = k_{f1}[M]^2 - (k_{r1} + k_2 + k_{f3}[I])[C_1] + k_{r3}[C_2] \tag{3}$$

$$\frac{\mathrm{d}[C_2]}{\mathrm{d}t} = k_{f3}[C_1][I] - (k_{r3} + k_4 + k_5[I])[C_2] \tag{4}$$

$$\frac{\mathrm{d}[C_3]}{\mathrm{d}t} = k_5[C_2][I] \tag{5}$$

$$\frac{\mathrm{d}[A]}{\mathrm{d}t} = k_2[C_1] + k_4[C_2] \tag{6}$$

Here, $[X]$ denotes the concentration of species X, and k_i are rate constants. The model's rate constants and initial concentrations represent specific physical processes. The rates k_{f1} and k_{r1} describe the forward and reverse reactions of primary nucleation. The parameters k_2 and k_4 govern the rate at which intermediate species transition to the final aggregate state. The core of the modulator's activity is captured by k_{f3}, which represents its binding rate to the C_1 complex, and k_5, which represents its rate of sequestration into the inactive C_3 sink.

2.1. Model simplification and non–dimensionalization

To analyze the system of ODEs, we simplified it through the techniques of timescale separation and nondimensionalization. To nondimensionalize the system, we used Kruskal's Principle of Minimum Simplification [27]. The core idea behind this principle is to choose scaling factors that simplify the least, maintaining a maximal set of comparable terms [28].

By invoking the quasi-steady state approximation (QSSA), we set the time-derivatives of the intermediate complexes to zero: $\mathrm{d}[C_1]/\mathrm{d}t = 0$ and $\mathrm{d}[C_2]/\mathrm{d}t = 0$. This approximation is valid given that the intermediate species are highly reactive and their concentrations change on a much faster timescale than the primary reactants, M and I [29, 30]. To simplify the analysis, we also applied a pseudo-first-order approximation (PFO), assuming the primary reactants' concentrations were not significantly depleted ($[M] \approx M_T$, $[I] \approx I_T$, where T denotes the total concentration) [31, 32]. The approximations $[M] \approx M_T$ and $[I] \approx I_T$ are reasonable for *in vitro* experiments where the total amount of protein and modulator is typically much larger than the concentration of reactive intermediates. The approximation $[I] \approx I_T$ holds true under two main conditions: either I is in large excess, or the binding affinity of I to form complexes is weak.

To demonstrate this claim, let us write down the mass conservation equation for species $[I]$. We have that the total concentration of inhibitor is equal to the sum of its concentrations in free and bound forms:

$$I_T = [I] + [C_2] + 2[C_3] \tag{7}$$

For the approximation $[I] \approx I_T$ to be valid, the concentration of bound I must be negligible compared to the total:

$$[C_2] + 2[C_3] \ll I_T$$

This condition is met in the following regimes:

1. **Large Excess of I ($I_T \gg M_T$)**: The total amount of complexes that can possibly form ($[C_1], [C_2], [C_3]$) is limited by the total amount of M, denoted M_T. If $I_T \gg M_T$, there simply is not enough M to create enough complexes to significantly deplete the large pool of free I.
2. **Weak Binding or Slow Sequestration (Large K_D)**: Even if I_T is not in large excess, $[I]$ can remain close to I_T if the complexes are unstable or form slowly. If $K_D = k_{r3}/k_{f3}$ is large (weak binding), C_2 will remain small. If $[C_2]$ is small, the rate of formation of C_3 (given by $k_5[C_2][I]$) will also be low, keeping $[C_3]$ small, especially on fast timescales.

The parameter regimes explored in our computational experiments are consistent with these conditions, particularly at high inhibitor concentrations (where the large excess condition applies) and low concentrations (where the amount of bound complex is minimal).

We can introduce dimensionless variables by scaling concentrations with their total values (M_T, I_T) and scaling time with the characteristic rate of monomer dimerization:

$$m = \frac{[M]}{M_T}, \quad i = \frac{[I]}{I_T}, \quad c_1 = \frac{[C_1]}{M_T}, \quad c_2 = \frac{[C_2]}{M_T}, \quad c_3 = \frac{[C_3]}{M_T}, \quad a = \frac{[A]}{M_T}, \tag{8a}$$

$$\tau = k_{f1} M_T t \tag{8b}$$

This yields a set of dimensionless parameters expressed as ratios of rate constants and initial concentrations:

$$\epsilon = \frac{M_T}{I_T}, \quad \alpha = \frac{k_{f3}}{k_{f1}}, \quad \beta = \frac{k_5}{k_{f1}}, \tag{9a}$$

$$\kappa_1 = \frac{k_{r1}}{k_{f1} M_T}, \quad \kappa_2 = \frac{k_2}{k_{f1} M_T}, \quad \kappa_3 = \frac{k_{r3}}{k_{f1} M_T}, \quad \kappa_4 = \frac{k_4}{k_{f1} M_T} \tag{9b}$$

Under the QSSA, we set $\mathrm{d}c_1/\mathrm{d}\tau = 0$ and $\mathrm{d}c_2/\mathrm{d}\tau = 0$, which yields the following algebraic system for the steady-state concentrations of the intermediates:

$$0 = m^2 - (\kappa_1 + \kappa_2 + \alpha/\epsilon) c_1 + \kappa_3 c_2 \tag{10}$$

$$0 = (\alpha/\epsilon) c_1 - (\kappa_3 + \kappa_4 + \beta/\epsilon) c_2 \tag{11}$$

Note that the above expressions, derived under the QSSA and nondimensionalization, depend on the approximation $i \approx 1$ (i.e., $[I] \approx I_T$).

From equation (11), we can solve for c_2 in terms of c_1:

$$c_2 = \frac{\alpha/\epsilon}{\kappa_3 + \kappa_4 + \beta/\epsilon} c_1 \equiv \Gamma \cdot c_1 \tag{12}$$

where we define

$$\Gamma = \frac{\alpha/\epsilon}{\kappa_3 + \kappa_4 + \beta/\epsilon} \tag{13}$$

Substituting equation (12) into equation (10) gives:

$$m^2 = (\kappa_1 + \kappa_2 + \alpha/\epsilon)c_1 - \kappa_3\Gamma c_1 = \left[(\kappa_1 + \kappa_2 + \alpha/\epsilon) - \kappa_3\Gamma\right] c_1 \tag{14}$$

Solving for c_1, we obtain:

$$c_{1,ss}(m) = K_{C1} \cdot m^2 \tag{15}$$

where

$$K_{C1} = \frac{1}{(\kappa_1 + \kappa_2 + \alpha/\epsilon) - \kappa_3\Gamma} \tag{16}$$

Using equations (12) and (15), we find:

$$c_{2,ss}(m) = \Gamma \cdot K_{C1} \cdot m^2 = K_{C2} \cdot m^2 \tag{17}$$

where

$$K_{C2} = \Gamma \cdot K_{C1} \tag{18}$$

The crucial insight from the analysis above is that the steady-state levels of the intermediates are directly proportional to the square of the free monomer concentration. The composite constants K_{C1} and K_{C2} encapsulate all the kinetic parameters and concentration ratios of the system.

This process reduces the system of differential equations for the intermediates to a solvable *algebraic* system, which allows us to express their dimensionless steady-state concentrations as functions of the monomer concentration m, as given by equations (15) and (17).

2.2. Steady states and dose-response

The ODE for the monomer concentration is of the form $\mathrm{d}m/\mathrm{d}\tau = -k_e m^2$, where $k_e = 2 - 2\kappa_1 K_{C1}$. The solution for the dimensionless monomer concentration is:

$$m(\tau) = \frac{m_0}{1 + m_0 k_e \tau} \tag{19}$$

Here, m_0 denotes the initial monomer concentration. Next, we substitute the solution for $m(\tau)$ into the ODE for a. Let $k_a = \kappa_2 K_{C1} + \kappa_4 K_{C2}$. The final solution for the dimensionless aggregate concentration is:

$$a(\tau) = a_0 + \frac{k_a m_0^2 \tau}{1 + m_0 k_e \tau} \tag{20}$$

2.3. Proof of structural hormesis

We proved that hormesis is a structural property of the model by analyzing the quasi-steady state rate of aggregation, $R = \mathrm{d}[A]/\mathrm{d}t$, as a function of the total inhibitor concentration, I_T. The analytical proof was performed with dimensional variables because it provides a more direct and intuitive link to the physical rate constants. Solving the algebraic system under the QSSA gives $R(I_T)$ as the following rational function:

$$R(I_T) = \frac{k_{f1} M_T^2 \left[k_2(k_{r3} + k_4) + (k_2 k_5 + k_4 k_{f3}) I_T\right]}{(k_{r1} + k_2)(k_{r3} + k_4) + \left[(k_{r1} + k_2)k_5 + k_{f3} k_4\right] I_T + (k_{f3} k_5) I_T^2} \tag{21}$$

The analysis proceeded in three steps:

1. **Limit as $I_T \to 0$:** In the absence of the modulator, the rate approaches a positive constant value, $R(0) > 0$.
2. **Limit as $I_T \to \infty$:** At high modulator concentrations, the numerator is of order I_T while the denominator is of order I_T^2. Therefore, the rate approaches zero: $\lim_{I_T \to \infty} R(I_T) = 0$.
3. **Initial Slope:** For hormesis to be manifest, the rate must initially increase. The derivative of a rational function $R(x) = N(x)/D(x)$ at $x = 0$ is positive if $N'(0)D(0) - N(0)D'(0) > 0$. For our rate $R(I_T)$, this term is:

$$
\begin{aligned}
&\{(k_2k_5 + k_4k_{f3}) \cdot (k_{r1} + k_2)(k_{r3} + k_4) - k_2(k_{r3} + k_4) \cdot [(k_{r1} + k_2)k_5 + k_{f3}k_4]\} \cdot k_{f1}M_T^2 \\
&= (k_{r3} + k_4)\,[(k_2k_5 + k_4k_{f3})(k_{r1} + k_2) - k_2((k_{r1} + k_2)k_5 + k_{f3}k_4)] \cdot k_{f1}M_T^2 \\
&= (k_{r3} + k_4)\,[k_2k_5(k_{r1} + k_2) + k_4k_{f3}(k_{r1} + k_2) - k_2k_5(k_{r1} + k_2) - k_2k_{f3}k_4] \cdot k_{f1}M_T^2 \\
&= (k_{r3} + k_4)\,[k_4k_{f3}k_{r1} + k_4k_{f3}k_2 - k_2k_{f3}k_4] \cdot k_{f1}M_T^2 \\
&= (k_{r3} + k_4)(k_4k_{f3}k_{r1}) \cdot k_{f1}M_T^2
\end{aligned}
$$

Since all rate constants (k_i) are positive real numbers, the initial slope is strictly positive. Because the rate function starts at a positive value, has a positive initial slope, and decays to zero at infinity, it is guaranteed to exhibit a maximum for $I_T > 0$. This proves that hormesis is a robust, structural property of the model, independent of specific parameter values. Although this proof analyzes the quasi-steady state rate of aggregation, our computational experiments in the next section focused on the final steady-state concentration of aggregate, $[A]$, which represents the most biologically relevant outcome (i.e., total pathological load).

3. Computational experiments

We simulated the model to determine the dose–response relationship between the total inhibitor concentration I_T and the total amount of aggregate A at steady-state. Numerical simulations showed a robust hormetic response and corroborated our analytical findings. Numerical integration of the systems was performed by the stiff solver LSODA in Python's SciPy library. All analyses were performed at steady-state with the parameter values shown in Tables 1 and 2. The parameter values for Figure 4A were taken from Rashkov et al. [17].

3.1. The Inhibitor Induces a Robust Hormetic Response

As shown in Figure 2, when the total inhibitor concentration (I_T) was low, the final concentration of aggregate (A) exceeded the basal level observed in the modulator's absence. As I_T increased further, this stimulatory effect reversed, and the amount of aggregate became strongly inhibited, eventually falling far below the basal level. For the parameters used in Figure 2, the basal level of aggregation (with $I_T = 0$) was approximately 0.0011 nM. At the peak of the hormetic curve ($I_T \approx 0.3$ nM), the aggregate concentration reached approximately 0.00175 nM. This represented a 1.6-fold increase compared to the basal level. This stimulatory effect reversed as the concentration of I_T increased further, leading to a profound inhibition of aggregation that fell far below the basal level.

We found that specific parameter values influenced the characteristics of the hormetic response, such as the magnitude and location of the peak. For instance, a higher sequestration

Table 1: Parameters for Figures 2 and 3

Parameter	Value	Units
$\boldsymbol{k_{f1}}$	1.11	$\mathrm{nmol^{-1}\,L^{-1}\,s^{-1}}$
$\boldsymbol{k_{r1}}$	8.56	$\mathrm{s^{-1}}$
$\boldsymbol{k_2}$	0.10	$\mathrm{s^{-1}}$
$\boldsymbol{k_{f3}}$	5.39	$\mathrm{nmol^{-1}\,L^{-1}\,s^{-1}}$
$\boldsymbol{k_{r3}}$	4.77	$\mathrm{s^{-1}}$
$\boldsymbol{k_4}$	8.23	$\mathrm{s^{-1}}$
$\boldsymbol{k_5}$	5.37	$\mathrm{nmol^{-1}\,L^{-1}\,s^{-1}}$
$\boldsymbol{M_T}$	5.00×10^{-3}	$\mathrm{nmol\,L^{-1}}$

Table 2: Parameters for Figure 4B

Parameter	Value	Units
Base case $\boldsymbol{k_2}$	0.10	$\mathrm{s^{-1}}$
High $\boldsymbol{k_2}$	1.00	$\mathrm{s^{-1}}$
Base case $\boldsymbol{k_4}$	8.23	$\mathrm{s^{-1}}$
Low $\boldsymbol{k_4}$	1.00	$\mathrm{s^{-1}}$

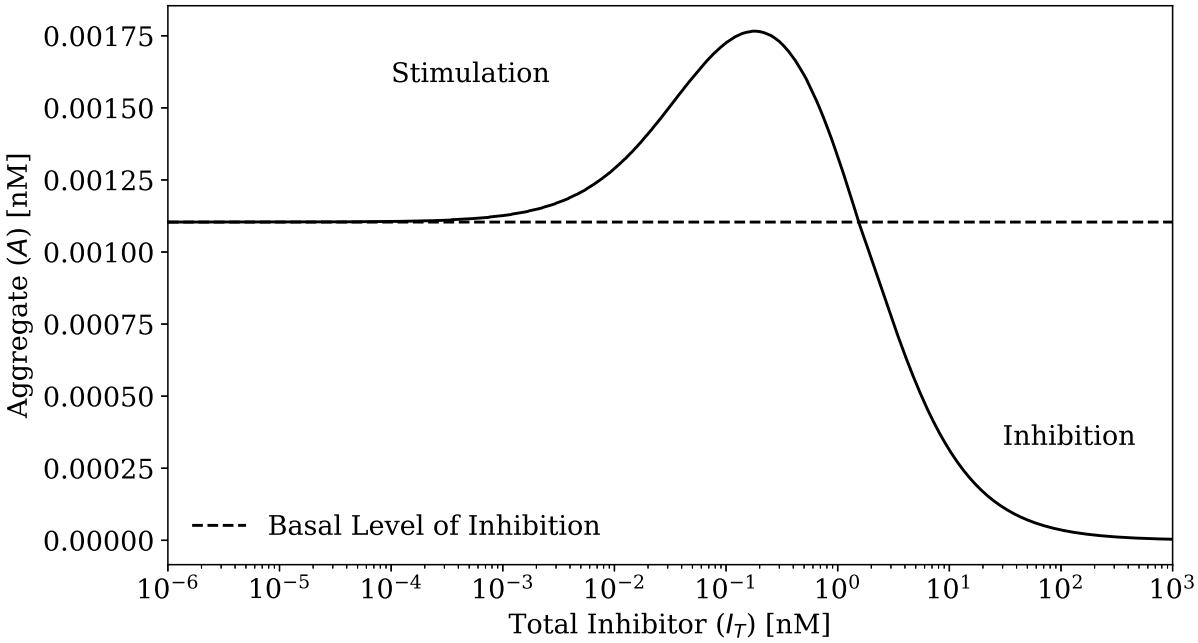

Figure 2: **Hormetic response of the aggregate to the inhibitory stimulus.** Dose–response of aggregate A at steady state as a function of total inhibitor I_T (logarithmic scale). Low doses stimulate aggregation, whereas high doses inhibit it, yielding a biphasic profile. The dashed line indicates the basal aggregate level without inhibitor. The parameter values used for the numerical simulations are available in Table 1.

rate (k_5) leads to a sharper decline in aggregation, shifting the inhibitory phase to a lower modulator concentration. This suggests that while the existence of the hormetic response is a structural property of the network, its specific quantitative features are tunable by kinetic parameters. This observation provides a smooth transition to our next section, where we demonstrate that the fundamental biphasic nature of the response is independent of these specific parameter values.

3.2. Intermediate Dynamics Drive the Hormetic Response

To understand the mechanism underlying this biphasic response, we analyzed the steady-state concentrations of the intermediate complexes C_1, C_2, and C_3 as a function of I_T (FIGURE 3). In the absence of the modulator, the system exists primarily as the C_1 complex. At low concentrations of I_T, C_1 is efficiently converted into C_2, the second productive intermediate. The rise in the concentration of C_2 directly corresponds to the region of stimulated aggregation shown in FIGURE 2. However, as I_T increases, the modulator's secondary action becomes dominant: C_2 is consumed to form the inactive C_3 complex. At high modulator concentrations, the system's effective mass is almost entirely sequestered in the C_3 state, effectively starving the productive pathway and causing profound inhibition of aggregation. Hormesis in this system is therefore a direct consequence of the inherent trade-off between the initial formation of the productive C_2 complex and its subsequent depletion into the inactive C_3 sink. Note that the apparent discontinuity at $I_T = 2$ nM is a key feature representing the underlying chemical kinetics of the system. This location marks the transition from a stimulation–dominated regime to an inhibition–dominated one, as seen in FIGURE 2.

3.3. Hormesis is an Intrinsic Structural Property of the Model

Finally, our analysis indicated that the observed hormetic response is a general feature of the model. In some biochemical systems, hormesis is parameter-dependent, emerging only when specific kinetic conditions are met (FIGURE 4A). To confirm our analytical result that this is not the case for our model, we performed simulations across a wide range of parameter sets, varying key rate constants by an order of magnitude. As shown in FIGURE 4B, the hormetic response was conserved in all cases. Although the magnitude and position of the peak response shifted, the fundamental biphasic shape remained. This result demonstrated that hormesis in this model is not a parameter-dependent phenomenon but rather an intrinsic and robust structural property of a network in which a modulator sequentially facilitates and then sequesters pathway intermediates. These findings present a novel mechanistic basis for hormesis in protein aggregation and caution that potential therapeutic inhibitors may have counterintuitive, pro-aggregating effects at low doses, underscoring the critical need for comprehensive dose–response evaluations in drug development and motivating targeted experimental studies to validate the proposed mechanism.

A comprehensive analysis of the parameter conditions governing the magnitude of the hormetic effect, including a phase diagram spanning three orders of magnitude in (k_2, k_4) space, is provided in Appendix Appendix A (see particularly Section Appendix A.3 and FIGURE A.5).

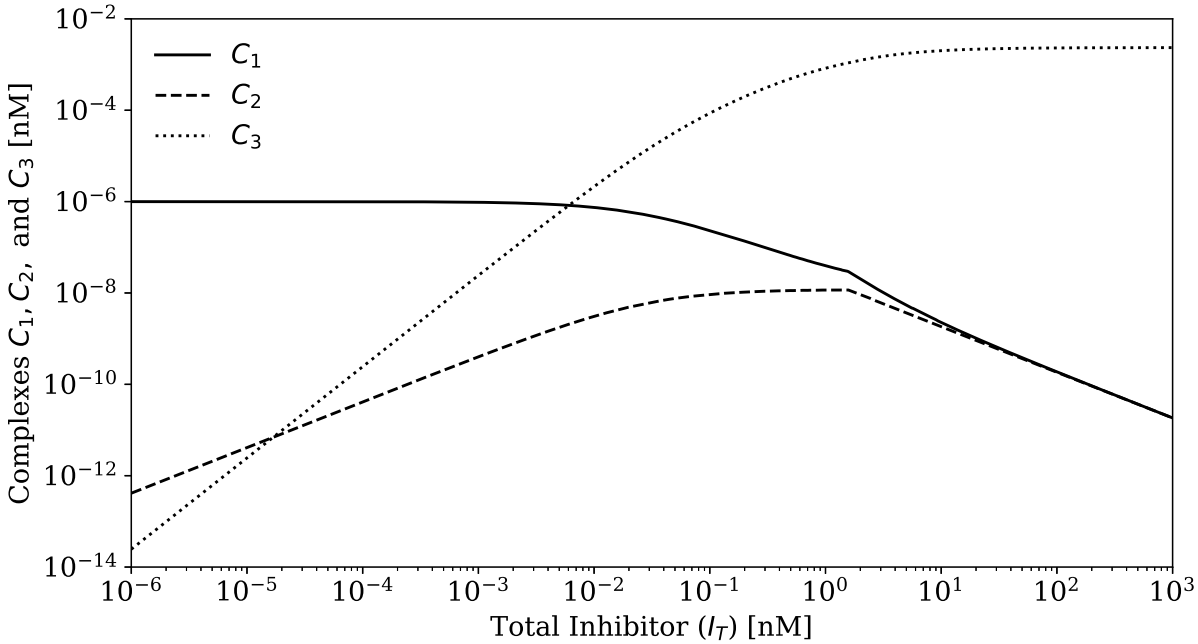

Figure 3: **Intermediate dynamics drive the hormetic response.** Intermediate complexes at steady state versus total inhibitor I_T (logarithmic axes). The rise of C_2 underlies the stimulatory portion, while the growth of the sink C_3 at high I_T depletes C_1/C_2 and produces the inhibitory portion. The parameters values used for numerical simulations are available in Table 1.

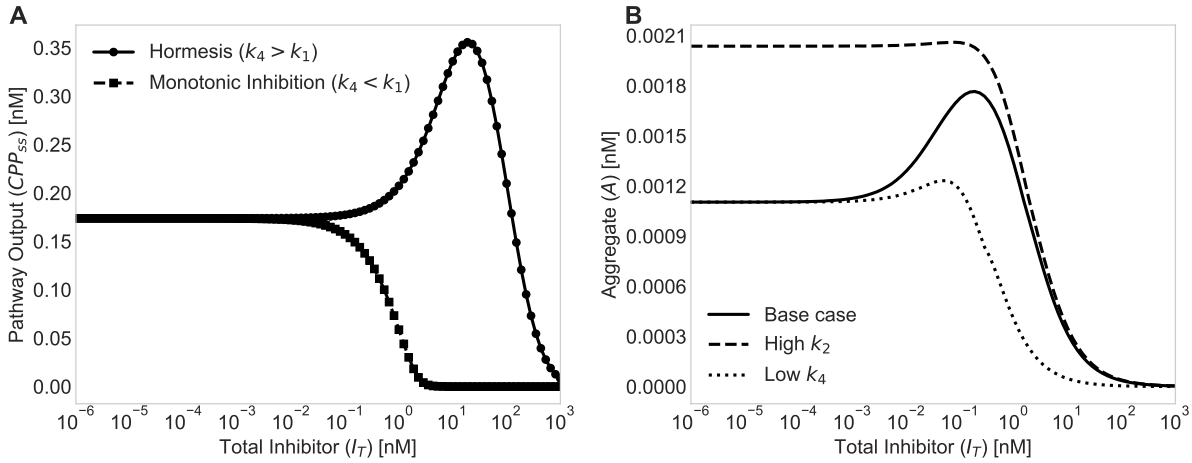

Figure 4: **Parameter–dependent versus structural hormesis.** (A) Simulation of the model by Rashkov et al. [17], where hormesis is parameter-dependent and conditional on specific kinetic parameters. Pathway output exhibits hormesis when $k_4 > k_1$ and monotonic inhibition when $k_4 < k_1$. (B) The biphasic shape of A versus I_T persists under order–of–magnitude perturbations of k_2 and k_4; peak location and amplitude shift but the response remains non–monotonic (simulations were carried out using the parameter sets in Tables 1 and 2). The biphasic hormetic response is conserved in all cases, confirming that it is an intrinsic structural property of the network topology.

4. Discussion

In this study, we developed and analyzed a mechanistic model of protein aggregation to investigate how the process is affected by a inhibitor. Our central finding is that this minimal, plausible reaction network for protein aggregation inherently produces a robust hormetic response. We demonstrated analytically that low concentrations of a inhibitor will paradoxically accelerate the rate of aggregation, while high concentrations are inhibitory. Crucially, this biphasic behavior is not contingent on a sensitive balance of kinetic parameters but is an intrinsic property of the model's structure, suggesting that hormesis may be a more common, yet overlooked, feature of protein aggregation kinetics than currently appreciated.

The origin of hormesis in our model can be traced to the dual role of the modulator, I. At low concentrations, its primary effect is to bind the initial complex C_1 and catalyze its conversion to the intermediate complex C_2. Since both C_1 and C_2 are on-pathway to forming the final aggregate A, and C_2 can be a productive species itself, this initial step can increase the overall flux through the aggregation pathway. However, as the concentration of I increases, its second function becomes dominant — the binding of the productive complex C_2 to form the irreversible, off-pathway complex C_3. This second binding event effectively sequesters material from the aggregation pathway, leading to potent inhibition at high doses. The biphasic response is therefore a direct consequence of this trade-off, where each effect dominates in a different concentration regime.

While our work builds upon previous studies of hormesis in biochemical networks, it also presents a key distinction. For example, a similar ODE-based approach has been used to show that kinase inhibition could lead to hormesis in a signaling cascade [17]. However, in their model, the emergence of hormesis was conditional, requiring a specific inequality between two rate constants. Our model reveals a different principle: that certain network topologies are inherently poised to generate a hormetic response. The sequential activation-inactivation motif in our model guarantees a biphasic response, suggesting that the structure of the network itself can be the primary determinant of such complex dynamics. This approach highlights the power of minimal, mechanistic models to reveal fundamental principles governing complex biological phenomena. By stripping away extraneous details, we can isolate the core network topology responsible for a specific behavior. This methodology, rooted in systems biology, is broadly applicable and can be used to investigate other paradoxical behaviors in diverse biological systems, from metabolic pathways and gene regulatory networks to enzyme kinetics. Furthermore, while broader studies have characterized the general nature of hormesis across many biological systems [7], our study provides a specific, bottom-up molecular mechanism that could plausibly underlie this phenomenon in the critical context of protein aggregation. Related network-level insights have also been observed in enzymatic systems showing biphasic dose–responses due to feedback control or substrate inhibition [7].

The implications of these findings for medicine and biotechnology are significant. The most profound consequence relates to the development of therapeutic inhibitors for neurodegenerative diseases characterized by protein aggregation. Our model predicts that a compound identified as a potent inhibitor in high-throughput screens (which are often performed at high concentrations) could paradoxically exacerbate the disease pathology at lower, more physiologically relevant doses. This highlights a potential pitfall in drug discovery and underscores the critical necessity of characterizing dose–response relationships over a wide

concentration range during preclinical development. Similar concerns have been raised in the context of drug-induced paradoxical effects observed in cancer therapies and neurological treatments [33]. Biologically, the modulator I could represent various factors, including small molecules, metal ions, or even molecular chaperones that have complex, concentration-dependent effects on protein conformation and assembly.

Our model is, by design, a simplified representation of a complex biochemical process. We have focused on a minimal network to isolate the core topology capable of producing structural hormesis. Key limitations of this coarse-grained approach include the representation of the aggregate pool A as a single species, which does not account for a distribution of aggregate sizes or for growth via monomer addition to existing aggregates [34]. Future extensions could incorporate such features, for instance by including an elongation step (e.g., $A + M \rightarrow A$). Additionally, limitations include the absence of competing cellular pathways, such as protein degradation by the ubiquitin-proteasome system. The model also assumes a well-mixed system and does not account for the complex spatiotemporal dynamics that can occur within a cell. Spatial heterogeneity and compartmentalization have been shown to influence aggregation kinetics *in vivo* [3, 35]. Future work should focus on extending the model to incorporate these additional layers of biological reality. The critical next step, however, is experimental validation. We hope our theoretical predictions will motivate experimental studies to systematically measure aggregation rates for proteins like amyloid-beta or alpha-synuclein across a broad spectrum of concentrations for various known modulators, to determine if the intrinsic hormetic response we describe here can be observed *in vitro* or *in vivo*.

To specifically test our model's predictions, we propose a dose–response study using the small molecule resveratrol to modulate amyloid-beta (Aβ) aggregation. Resveratrol's effects on Aβ have been shown to be complex and concentration-dependent, including inhibiting oligomeric cytotoxicity without preventing oligomer formation [36] and even mediating the cleavage of the peptide into smaller fragments [37]. A straightforward *in vitro* experiment could be performed by incubating the Aβ protein with a wide range of resveratrol concentrations and then using a common fluorescent assay, such as Thioflavin T (ThT), to measure the amount of aggregate formed [38]. The direct binding of resveratrol to both monomeric and fibrillar Aβ has been previously demonstrated [39]. Our model predicts that the resulting dose–response curve would be bell–shaped, demonstrating a hormetic effect where low concentrations of resveratrol increase aggregation, while higher concentrations inhibit it. This outcome would provide direct experimental evidence for the proposed activation–inactivation mechanism.

Data accessibility

All Python code and simulation data supporting this publication are publicly available at `https://doi.org/10.5281/zenodo.18370730`.

CRediT Authors' contributions

Abhishek Mallela: Data curation, Formal analysis, Investigation, Methodology, Visualization, Writing – original draft, review & editing. **Santiago Schnell:** Conceptualization,

Funding Acquisition, Investigation, Methodology, Project administration, Resources, Supervision, Writing – review & editing.

Competing interests

The authors declare no competing interests.

Funding

This work was partially funded by Dartmouth.

References

[1] C. Soto, Unfolding the role of protein misfolding in neurodegenerative diseases, Nature Reviews Neuroscience 4 (2003) 49–60. doi:10.1038/nrn1007.

[2] F. Chiti, C. M. Dobson, Protein misfolding, functional amyloid, and human disease, Annual Review of Biochemistry 75 (2006) 333–366. doi:10.1146/annurev.biochem.75.101304.123901.

[3] T. P. J. Knowles, M. Vendruscolo, C. M. Dobson, The amyloid state and its association with protein misfolding diseases, Nature Reviews Molecular Cell Biology 15 (2014) 384–396. doi:10.1038/nrm3810.

[4] J. Habchi, P. Arosio, M. Perni, A. R. Costa, S. Youssef, C. Galvagnion, T. C. T. Michaels, M. Casford, D. A. Comfort, F. Taddei, S. Linse, C. M. Dobson, T. P. J. Knowles, M. Vendruscolo, An anticancer drug suppresses the primary nucleation reaction that initiates the production of the toxic $\beta 42$ aggregates linked with Alzheimer's disease, Science Advances 2 (2016) e1501244. doi:10.1126/sciadv.1501244.

[5] T. C. T. Michaels, P. Arosio, T. P. J. Knowles, Thermodynamic and kinetic design principles for amyloid-aggregation inhibitors, Proceedings of the National Academy of Sciences 117 (2020) 24251–24257. doi:10.1073/pnas.2006684117.

[6] E. J. Calabrese, L. A. Baldwin, The frequency of U-shaped dose responses in the toxicological literature, Toxicological Sciences 62 (2001) 330–338. doi:10.1093/toxsci/62.2.330.

[7] E. J. Calabrese, Hormesis: Why it is important to toxicology and toxicologists, Environmental Toxicology and Chemistry 27 (2008) 1451–1474. doi:10.1897/07-541.1.

[8] S. Tang, R. A. Cheke, Y. Xiao, A general model of hormesis in biological systems and its application to pest management, Journal of The Royal Society Interface 16 (2019) 20190468. doi:10.1098/rsif.2019.0468.

[9] M. P. Mattson, Hormesis defined, Ageing Research Reviews 7 (2008) 1–7. doi:10.1016/j.arr.2007.08.007.

[10] A. R. D. Stebbing, Hormesis — The stimulation of growth by low levels of inhibitors, Science of the Total Environment 22 (1982) 213–234. doi:10.1016/0048-9697(82)90066-3.

[11] U. Alon, An Introduction to Systems Biology: Design Principles of Biological Circuits, Chapman and Hall/CRC, 2006. doi:10.1201/9781420011432.

[12] E. D. Sontag, Dynamic compensation, parameter identifiability, and equivariances, PLoS Computational Biology 13 (2017) e1005447. doi:10.1371/journal.pcbi.1005447.

[13] C. Kumsta, J. T. Chang, J. Schmalz, M. Hansen, Hormetic heat stress and HSF-1 induce autophagy to improve survival and proteostasis in *C. elegans*, Nature Communications 8 (2017) 14337. doi:10.1038/ncomms14337.

[14] L. Matai, G. C. Sarkar, M. Chamoli, Y. Malik, S. S. Kumar, U. Rautela, N. R. Jana, K. Chakraborty, A. Mukhopadhyay, Dietary restriction improves proteostasis and increases life span through endoplasmic reticulum hormesis, Proceedings of the National Academy of Sciences 116 (2019) 17383–17392. doi:10.1073/pnas.1900055116.

[15] N. Katyal, M. Agarwal, R. Sen, V. Kumar, S. Deep, Paradoxical Effect of Trehalose on the Aggregation of α-Synuclein: Expedites Onset of Aggregation yet Reduces Fibril Load, ACS Chemical Neuroscience 9 (2018) 1477–1491. doi:10.1021/acschemneuro.8b00056.

[16] C. A. Waudby, T. P. Knowles, G. L. Devlin, J. N. Skepper, H. Ecroyd, J. A. Carver, M. E. Welland, J. Christodoulou, C. M. Dobson, S. Meehan, The Interaction of αB-Crystallin with Mature α-Synuclein Amyloid Fibrils Inhibits Their Elongation, Biophysical journal 98 (2010) 843–851. doi:10.1016/j.bpj.2009.10.056.

[17] P. Rashkov, I. P. Barrett, R. E. Beardmore, C. Bendtsen, I. Gudelj, Kinase inhibition leads to hormesis in a dual phosphorylation-dephosphorylation cycle, PLoS Computational Biology 12 (2016) e1005216. doi:10.1371/journal.pcbi.1005216.

[18] A. Mallela, A. Hastings, The role of stochasticity in noise-induced tipping cascades: A master equation approach, Bulletin of Mathematical Biology 83 (2021) 1–20. doi:10.1007/s11538-021-00889-1.

[19] F. Oosawa, M. Kasai, A theory of linear and helical aggregations of macromolecules, Journal of Molecular Biology 4 (1962) 10–21. doi:10.1016/S0022-2836(62)80112-0.

[20] F. A. Ferrone, Analysis of protein aggregation kinetics, Methods in Enzymology 309 (1999) 256–274. doi:10.1016/s0076-6879(99)09019-9.

[21] T. P. J. Knowles, C. A. Waudby, G. L. Devlin, S. I. A. Cohen, A. Aguzzi, M. Vendruscolo, E. M. Terentjev, M. E. Welland, C. M. Dobson, An analytical solution to the kinetics of breakable filament assembly, Science 326 (2009) 1533–1537. doi:10.1126/science.1178250.

[22] S. I. Cohen, S. Linse, L. M. Luheshi, E. Hellstrand, D. A. White, L. Rajah, D. E. Otzen, M. Vendruscolo, C. M. Dobson, T. P. Knowles, Proliferation of amyloid-β42 aggregates occurs through a secondary nucleation mechanism, Proceedings of the National Academy of Sciences 110 (2013) 9758–9763. doi:10.1073/pnas.1218402110.

[23] G. Meisl, J. B. Kirkegaard, P. Arosio, T. C. T. Michaels, M. Vendruscolo, C. M. Dobson, S. Linse, T. P. J. Knowles, Molecular mechanisms of protein aggregation from global fitting of kinetic models, Nature Protocols 11 (2016) 252–272. doi:10.1038/nprot.2016.010.

[24] G. Meisl, T. P. Knowles, D. Klenerman, The molecular processes underpinning prion-like spreading and seed amplification in protein aggregation, Current Opinion in Neurobiology 61 (2020) 58–64. doi:10.1016/j.conb.2020.01.010.

[25] A. M. Morris, M. A. Watzky, R. G. Finke, Protein aggregation kinetics, mechanism, and curve-fitting: a review of the literature, Biochimica et Biophysica Acta – Proteins and Proteomics 1794 (2009) 375–397. doi:10.1016/j.bbapap.2008.10.016.

[26] M. Whidden, A. Ho, M. I. Ivanova, S. Schnell, Competitive inhibition reaction mechanisms for the two-step model of protein aggregation, Biophysical Chemistry 193–194 (2014) 9–19. doi:10.1016/j.bpc.2014.06.006.

[27] M. Kruskal, Asymptotology, in: Lectures presented at the Trieste Seminar on Plasma Physics, 1965, p. 373.

[28] S. Shoffner, S. Schnell, Approaches for the estimation of timescales in nonlinear dynamical systems: Timescale separation in enzyme kinetics as a case study, Mathematical biosciences 287 (2017) 122–129. doi:10.1016/j.mbs.2016.09.001.

[29] J. Eilertsen, S. Schnell, S. Walcher, Natural parameter conditions for singular perturbations of chemical and biochemical reaction networks, Bulletin of Mathematical Biology 85 (2023) 48. doi:10.1007/s11538-023-01150-7.

[30] J. Eilertsen, S. Schnell, S. Walcher, Rigorous estimates for the quasi-steady state approximation of the Michaelis–Menten reaction mechanism at low enzyme concentrations, Nonlinear Analysis: Real World Applications 78 (2024) 104088. doi:10.1016/j.nonrwa.2024.104088.

[31] S. Schnell, C. Mendoza, The condition for pseudo-first-order kinetics in enzymatic reactions is independent of the initial enzyme concentration, Biophysical Chemistry 107 (2004) 165–174. doi:10.1016/j.bpc.2003.09.003.

[32] J. Eilertsen, S. Schnell, S. Walcher, The michaelis–menten reaction at low substrate concentrations: Pseudo-first-order kinetics and conditions for timescale separation, Bulletin of Mathematical Biology 86 (2024) 68. doi:10.1007/s11538-024-01295-z.

[33] A. Aguzzi, T. O'Connor, Protein aggregation diseases: Pathogenicity and therapeutic perspectives, Nature Reviews Drug Discovery 9 (2010) 237–248. doi:10.1038/nrd3050.

[34] S. Shoffner, S. Schnell, Estimation of the lag time in a subsequent monomer addition model for fibril elongation, Physical Chemistry Chemical Physics 18 (2016) 21259–21268. doi:10.1039/C5CP07845H.

[35] A. Patel, L. Malinovska, S. Saha, J. Wang, S. Alberti, D. Drechsel, A. A. Hyman, ATP as a biological hydrotrope, Science 356 (2017) 753–756. doi:10.1126/science.aaf6846.

[36] Y. Feng, X.-p. Wang, S.-g. Yang, Y.-j. Wang, X. Zhang, X.-t. Du, X.-x. Sun, M. Zhao, L. Huang, R.-t. Liu, Resveratrol inhibits beta-amyloid oligomeric cytotoxicity but does not prevent oligomer formation, Neurotoxicology 30 (2009) 986–995. doi:10.1016/j.neuro.2009.08.013.

[37] S. Al-Edresi, H. A. El-Serehy, S. R. Ede, A. A. Amini, N. H. Al-Rikabi, S. Al-Edresi, Resveratrol-mediated cleavage of amyloid β_{1-42} peptide: Potential relevance to Alzheimer's disease, Neurobiology of Aging 94 (2020) 24–33. doi:10.1016/j.neurobiolaging.2020.04.012.

[38] H. R. Ahn, H. A. Chung, Y. M. Sung, Y. S. Ha, B. S. Kim, Y. S. Yoo, J. Y. Kim, Novel method for quantitative determination of amyloid fibrils of alpha-synuclein and amyloid β/A4 protein by using resveratrol, Analytical Biochemistry 367 (2007) 259–261. doi:10.1016/j.ab.2007.05.023.

[39] J.-F. Ge, J.-P. Qiao, C.-C. Qi, C.-W. Wang, J.-N. Zhou, The binding of resveratrol to monomer and fibril amyloid beta, Neurochemistry International 61 (2012) 1192–1201. doi:10.1016/j.neuint.2012.08.012.

Appendix A. Parameter-dependent and independent hormesis

Appendix A.1. Parameter-dependent hormesis in the model of Rashkov et al.

Rashkov et al. [17] analyzed a dual phosphorylation-dephosphorylation cycle in which a kinase inhibitor can produce hormetic responses in pathway output. In their model, hormesis is a *parameter-dependent* phenomenon: the biphasic response emerges only when the dephosphorylation rate k_4 exceeds the phosphorylation rate k_1 (i.e., $k_4 > k_1$). When this inequality is reversed ($k_4 < k_1$), the system exhibits monotonic inhibition.

The mathematical basis for this condition can be understood as follows. In their model, the inhibitor acts on the kinase, reducing phosphorylation flux. When the rate of dephosphorylation is fast relative to the rate of phosphorylation ($k_4 > k_1$), low inhibitor concentrations create a kinetic regime in which the substrate accumulates in an intermediate phosphorylated state that contributes to pathway output, producing transient stimulation. When phosphorylation dominates ($k_4 < k_1$), inhibition of the kinase immediately reduces flux through the pathway at all concentrations.

Appendix A.2. Structural versus practical hormesis in the aggregation model

In contrast to the model of Rashkov et al. [17], we proved analytically (Section 2.3) that the initial slope of the aggregation rate $R(I_T)$ with respect to inhibitor concentration is *always positive* for any choice of positive rate constants:

$$\left.\frac{dR}{dI_T}\right|_{I_T=0} = \frac{(k_{r3}+k_4)(k_4 k_{f3} k_{r1}) \cdot k_{f1} M_T^2}{[(k_{r1}+k_2)(k_{r3}+k_4)]^2} > 0 \tag{A.1}$$

This guarantees that hormesis is a *structural* property of the network topology: the rate function must have a maximum at some $I_T > 0$.

However, the *magnitude* of the hormetic effect—quantified by the ratio of peak aggregate concentration to baseline aggregate concentration—depends on the relative values of the rate constants. When the direct aggregation pathway ($C_1 \to A$ via k_2) dominates the inhibitor-mediated pathway ($C_2 \to A$ via k_4), the hormetic peak becomes vanishingly small and may be practically undetectable.

Appendix A.3. Phase diagram analysis of parameter space

To characterize the parameter regimes where hormesis is practically significant, we computed the hormesis ratio (peak aggregate concentration divided by baseline aggregate concentration) across a two-dimensional grid of k_2 and k_4 values spanning three orders of magnitude (10^{-4} to 10^{-1} s^{-1}). Figure A.5 presents the resulting phase diagram.

The key findings are as follows:

1. **Hormetic region**: When $k_2 < k_{2,c}$, where $k_{2,c} \approx 0.045$ s^{-1}, the hormesis ratio substantially exceeds unity, indicating pronounced biphasic behavior. Notably, this boundary is largely independent of k_4, as evidenced by the nearly vertical transition in the phase diagram.
2. **Monotonic regime**: When $k_2 > k_{2,c}$, the direct pathway dominates, and the hormesis ratio approaches unity. In this regime, the mathematically guaranteed positive initial slope produces a hormetic peak small enough as to be experimentally undetectable.

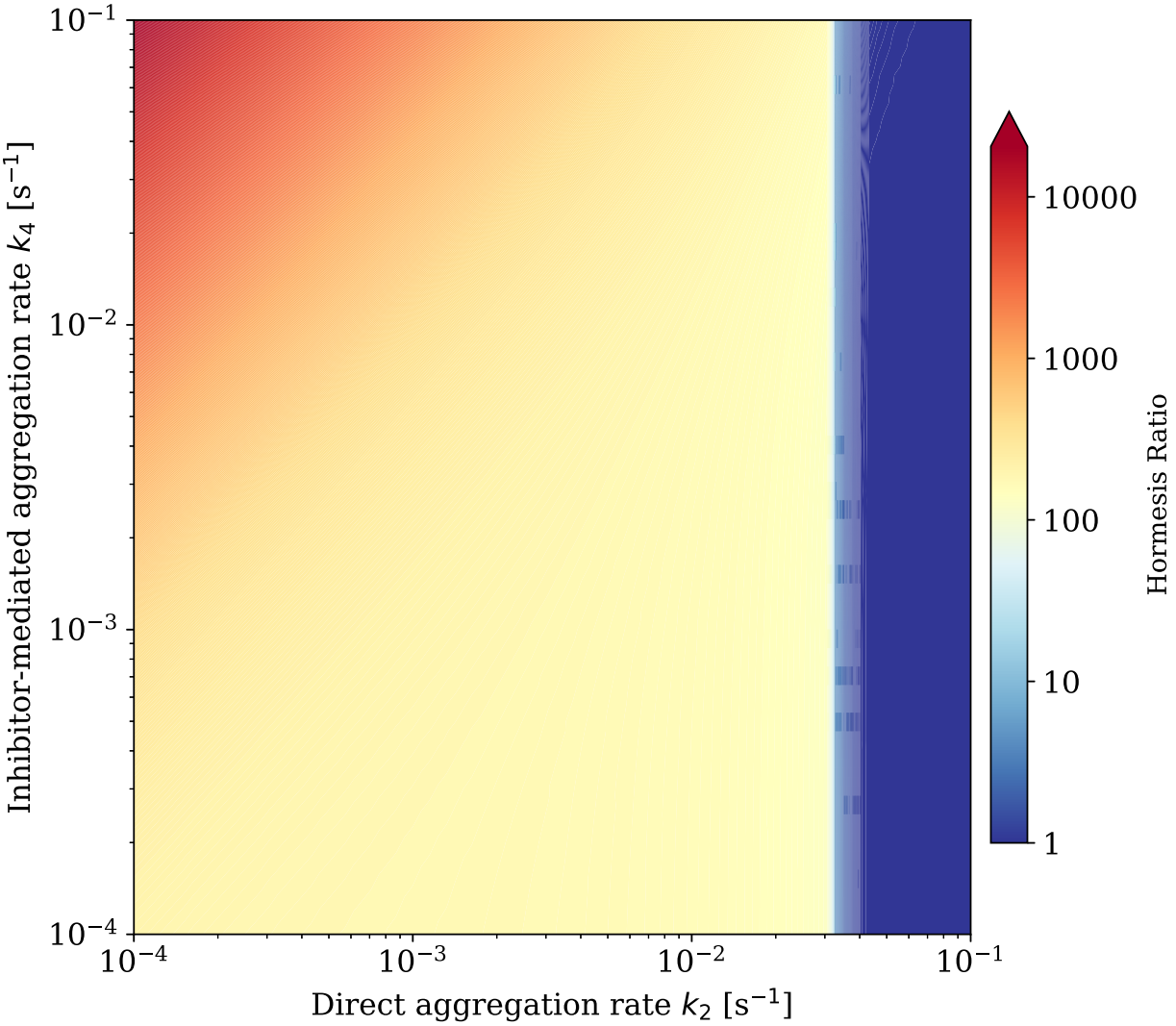

Figure A.5: **Phase diagram of hormesis.** Heat map of the hormesis ratio—the maximum steady-state aggregate concentration divided by the baseline (inhibitor-free) concentration—across a 100×100 grid in the (k_2, k_4) parameter space. The direct aggregation rate k_2 ($C_1 \to A$) varies along the horizontal axis; the inhibitor-mediated rate k_4 ($C_2 \to A$) varies along the vertical axis. Both rates span from 10^{-4} to 10^{-1} s^{-1} on logarithmic scales. There is a marked transition from pronounced hormesis (warm colors, ratio > 1) to effectively monotonic inhibition (cool colors, ratio ≈ 1). **Methods:** For each (k_2, k_4) pair, the ODE system (Equations 1–6) was integrated using the stiff solver LSODA with relative and absolute tolerances of 10^{-12} for 75 logarithmically–spaced inhibitor concentrations ($I_T = 10^{-6}$ to 10^3 nM). Quasi-steady state was defined as convergence of all state variables to within a tolerance of 10^{-6} over successive 10-second integration intervals. This criterion captures the kinetically relevant quasi-steady state where hormesis manifests, rather than the true thermodynamic equilibrium where hormesis disappears. Computations were parallelized using the `joblib` library in Python.

Appendix A.4. Mechanistic interpretation

The condition $k_2 < k_{2,c}$ for practical hormesis has a clear mechanistic interpretation. For the inhibitor to produce a stimulatory effect at low concentrations, the direct aggregation pathway ($C_1 \to A$) must be sufficiently slow that the inhibitor-mediated pathway through

C_2 can make a substantial contribution to aggregate formation. When the direct pathway is fast ($k_2 > k_{2,c}$), aggregate forms primarily via $C_1 \to A$ before the inhibitor can redirect flux through C_2.

The near-independence of this threshold from k_4 indicates that the critical factor is not how fast C_2 produces aggregate, but rather whether C_2 has sufficient opportunity to form at all. When k_2 exceeds the critical value, C_1 is depleted so rapidly via the direct pathway that inhibitor binding cannot effectively compete, regardless of how productive the $C_2 \to A$ step might be.

Appendix A.5. Comparison with the model of Rashkov et al.

The key distinction between the two models is summarized in Table A.3:

Property	**Model of Rashkov et al.**	**Aggregation model**
Hormesis type	Parameter–dependent	Structural
Condition for hormesis	$k_4/k_1 > 1$ (strict)	$k_2 < k_{2,c}$ (practical)
Behavior when violated	Monotonic inhibition	Negligible hormesis
Mathematical guarantee	None	Positive initial slope

Table A.3: Comparison of parameter conditions for hormesis. With the parameter range examined in our aggregation model, the critical value $k_{2,c} \approx 0.045$ s^{-1} is largely independent of k_4.

In the Rashkov model, hormesis is a binary phenomenon—it either occurs or does not, depending on whether the parameter inequality is satisfied. In our aggregation model, hormesis is mathematically guaranteed but its practical significance depends primarily on whether k_2 falls below the critical threshold $k_{2,c} \approx 0.045$ s^{-1}.